Electrical double layer capacitors with sucrose derived carbon electrodes in ionic liquid electrolytes

Lu Wei [a,b], G. Yushin [a,*]

[a] School of Materials Science and Engineering, Georgia Institute of Technology, Atlanta, GA 30332, USA
[b] C/C Composites Research Center, National Key Laboratory of Thermostructure Composite Materials, Northwestern Polytechnical University, Xi'an, Shaanxi 710072, PR China

ABSTRACT

Activated carbons were prepared via a pyrolysis of sucrose followed by activation in the stream of CO_2 gas for 2–6 h at 900 °C to tune the pore size distribution (PSD) and increase the specific surface area (SSA). The porosity of the activated sucrose derived carbons (ASCs) has been characterized using N_2 sorption measurements. Increasing activation time led to the significant increase in SSA and pore volume of ASCs, among which sucrose derived carbon with 6 h activation time (ASC-6 h) exhibited the highest SSA of 1941 $m^2 g^{-1}$ and the highest micropore volume of 0.87 $cm^3 g^{-1}$. Cyclic voltammetry (CV), electrochemical impedance spectroscopy (EIS) and galvanostatic charge–discharge cycle tests have been applied to investigate the capacitive performance of the ASC electrodes in ionic liquids (ILs) at room and elevated temperatures. The ASC-6 h electrodes in ethyl-dimethyl-propyl-ammonium bis (trifluoromethylsulfonyl) imide (EdMPNTf_2N) showed specific capacitance in excess of 170 $F g^{-1}$ at 60 °C, whereas the same electrodes in 1-ethyl-3-methylimidazolium tetrafluoroborate ($EMImBF_4$) showed slightly lower capacitance but significantly better rate performance.

© 2011 Elsevier B.V. All rights reserved.

1. Introduction

The development of energy-sustainable and energy-efficient economy depends on the ability to produce novel renewable materials for electrical energy storage devices. The electrical double layer capacitors (EDLCs) have attracted considerable attention because of their high power density, long cycling durability (in excess of 500,000 charge–discharge cycles) and charging within tens of seconds [1,2]. EDLCs applications range from memory back-up systems, uninterruptable power supplies, smart grid applications, and very importantly hybrid electric vehicles (HEVs) by coupling with fuel cells or secondary batteries to deliver high power for vehicle acceleration and store the energy converted from braking [1,3,4]. The demanding applications require further increase in the energy density of EDLC technology [5] with simultaneous decrease in cost and enhancements in safety. In addition, selected applications require high operating temperature (≥60 °C). Since the energy of an EDLC is proportional to the square of the highest operational voltage, the application of high voltage electrolytes leads to a significant enhancement of EDLCs' energy density. Replacing the aqueous electrolytes with organic electrolytes allows increase in the operating voltage by up to 3 times. However, organic solvents

do not meet the highly desired requirements of environmental compatibility and safety, because organic solvents exhibit high vapor pressure, suffer from inherent flammability and potential explosion risks. Compared with aqueous and organic electrolytes, ionic liquids (ILs) are more suitable for HEV applications [6] due to their high thermal stability, very low vapor pressure, wider electrochemical stability window and excellent performance at high temperatures [7–12]. Several ILs having high dielectrical permittivity combined with relatively high ionic conductivity and low viscosity at <60 °C, including 1-ethyl-3-methylimidazolium tetrafluoroborate ($EMImBF_4$) [7,13] and ethyl-dimethyl-propyl-ammonium bis (trifluoromethylsulfonyl) imide ($EdMPNTf_2N$), may show particular promises in EDLCs.

Porous carbons with their relatively low price, high electrical conductivity and high specific surface area (SSA) are used in commercial EDLCs. The electrochemical performance of EDLC carbon electrodes strongly depends on the structural parameters of porous carbon, such as the SSA [14–19], pore size [14–16], pore tortuosity [17,18], surface chemistry of carbon [20–24], and the size of carbon particles [25], among a few. The pores smaller than the ion size or highly tortuous pores with bottle-necks may prevent the access of the electrolyte ions to the pore surface and result in a low capacitance and/or slow frequency response. Therefore, it is important to design carbon materials with pores large enough for the electrolyte ions to access freely, but in the meantime, small enough to ensure a large surface area, high volumetric and gravimetric specific capacitance [14–16]. Various carbon materials, including activated

* Corresponding author at: 771 Ferst Dr. NW, Room 371, Atlanta, GA 30332-0245, USA. Tel.: +1 404 385 3261; fax: +1 404 894 9140.
E-mail address: yushin@gatech.edu (G. Yushin).

carbons (ACs) [26], carbide-derived carbons (CDCs) [7,9], carbon nanotubes (CNTs) [27,28], and carbon gels (CGs) [8], have been investigated as electrode materials for IL-based EDLCs. CNTs and macroporous CGs [8,27,28] with large external surface area commonly offer high rate capability but low capacitance per unit mass and volume. Vertically aligned CNTs [27] can deliver high specific capacitance and power density after plasma-etching treatment, but the preparation requires complicated synthesis procedure. CDC [14,29,30] offer good pore size control and exhibit attractive properties [14], but their production is very limited. In spite of the significant competition, ACs with their large production volumes and low cost still remain the choice for commercial EDLCs and many other applications. Recent progress in AC synthesis [20,21] shows that a classical porous carbon synthesis route via pyrolysis of organic compounds followed by activation will likely remain a viable commercial solution.

The growing global energy demand and an increased awareness of the environmental impacts of fossil fuel combustion led to the ACs production from natural materials, such as coconut shells [31], cotton [32], and other agricultural [33,34] and forest residues [35]. In the view of the authors, sugars (sucrose) could be particularly attractive AC precursors due to their uniform structure (and thus uniform and reproducible properties of the produced ACs, critically important property for EDLC manufacturers), very low price, local availability and high chemical purity. Surprisingly, sugar-derived ACs have received little-to-no attention as perspective materials for EDLCs.

The pore size and the SSA of the carbonized precursors can be increased by using physical and chemical activation methods. While chemical activation may lead to higher SSA and more uniform pores, it introduces metal ions into the AC, which are challenging and expensive to remove with post-processing. Compared with chemical activation, physical activation using carbon dioxide (CO_2) or steam is simpler and environmentally friendlier process, which has lower cost and does not introduce impurities. If improved synthesis conditions would allow the fabrication of better performing AC, the low cost and environment friendly sugar-derived carbon might be considered for the new generation of commercial EDLCs.

In this paper, we report on the formation of AC by pyrolysis and subsequent activation of sucrose. By controlling the activation time, high SSA and well developed microporosity was obtained. The microstructure of the activated sucrose-derived carbons (ASCs) and their electrochemical performances at various temperature and current densities in EDLCs with $EMImBF_4$ and $EdMPNTf_2N$ IL electrolytes have been studied.

2. Experimental

2.1. Activated carbon preparation

Sucrose, de-ionized (DI) water and sulfuric acid (H_2SO_4) were mixed with mass fraction of 1:0.5:0.1 (4 g of sucrose, 2 g of DI water and 0.4 g of H_2SO_4 in one batch) to form an aqueous sucrose/catalyst solution. The solution was pre-heat-treated in a tube furnace under Ar gas (99.9%, Air Gas, USA) flow at 70 °C for 2 h, and then it was heated to 700 °C at a heating rate of 10 °C min^{-1} and carbonized for 2 h. After carbonization, the solid carbon samples were cooled down to room temperature under an Ar flow and grinded using a QM-3SP04 planetary ball mill (Across International, USA) at a speed of 400 rpm for 3 h to produce carbon powder. The powders were subsequently heated to 900 °C under an Ar flow and activated using a pure CO_2 gas (99.9%, Air Gas, USA) for 2, 4 and 6 h, respectively. The samples were then cooled under an Ar flow in order to minimize the possible formation of surface groups at elevated temperatures.

These carbon samples are denoted as ASC-2 h, ASC-4 h and ASC-6 h with reference to different activation time.

2.2. Carbon characterization

The morphologies of as-prepared carbons materials were observed via a Leo 1530 (LEO, Osaka, Japan, now Nano Technology Systems Division of Carl Zeiss SMT, USA) scanning electron microscope (SEM). The carbons were characterized by N_2 adsorption/desorption measurements at −196 °C and CO_2 adsorption at 0 °C using a TriStar II 3020 surface area and porosity analyzer (Micromeritics Instrument Corporation, USA). Before the sorption analyses, the carbon samples were degassed at 300 °C using the VacPrep 061 Degasser (Micromeritics Instrument Corporation, USA) to remove moisture and other adsorbed contaminants. The SSAs were calculated from N_2 adsorption isotherms using the Brunauer–Emmett–Teller (BET) equation. Pore size distributions (PSDs) were calculated by the density functional theory (DFT) methods for N_2 and CO_2 adsorption in carbon slit pores.

2.3. Device assembly

Electrodes were prepared by mixing 92 wt. % activated carbon (AC) and 8 wt. % polytetrafluoroethylene (PTFE) in ethanol to form slurry. The slurry was stirred uniformly and at the same time heated on a hot plate at 150 °C to evaporate most of the ethanol and form a plasticine-like material. The produced AC-PTFE composite was then rolled to ~300 μm thick carbon sheet electrode. The electrode was placed into a vacuum oven (100 °C) overnight to remove moisture and residual hydrocarbons, and then was cut into round shape in the diameter of 12.7 mm for EDLC electrodes. 2016 stainless-steel coin cells with two symmetrical carbon electrodes separated by two GORE^{TM} PTFE separators (W.L. Gore and Associates, USA) of ~25 μm in thickness and ~60% porosity were assembled inside an Ar-filled glove box (<1 ppm of oxygen and H_2O, Innovation Technology, USA). Al foil of 300 μm in thickness roughened using a 600 grit SiC sandpaper and spray-coated with a thin layer (~10–20 μm) of graphite coating (grade BW 525, Superior Graphite, USA) was attached to each electrode and served as a current collector. The graphite coating was used to reduce the interfacial resistance between the electrode and the current collector. Two kinds of ionic liquids were selected as electrolytes: $EMImBF_4$ and $EdMPNTf_2N$ (purity >98%, Ionic Liquids Technology, Germany). While $EMImBF_4$ has been studied in EDLC applications [7,13], we could not find reports on the use of $EdMPNTf_2N$. Their main physicochemical properties [36,37] are shown in Table 1.
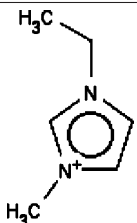
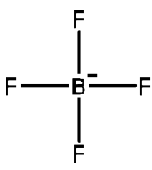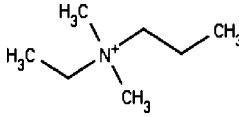### 2.4. Electrochemical testing

Cyclic voltammetry (CV) studies were performed using a Solartron 1480A MultiStat (Solartron Analytical, UK) in the voltage range −2.3 V to +2.3 V and in scan rates from 1 to 500 mV s^{-1}. The gravimetric capacitance, C (F g^{-1}), was calculated according to

$$C = \frac{2I}{(dV/dt)m}$$

where I is the current (A), dV/dt is the scan rate (V s^{-1}), and m is the mass of carbon in each electrode (g).

Electrochemical impedance spectroscopy (EIS) measurements were carried out using an IM6ex electrochemical workstation (Zahner-Elektrik, Germany) in the frequency range of 1 mHz–100 kHz with a 10 mV AC amplitude. The gravimetric capac-

Table 1
Physicochemical characteristics of EMImBF$_4$ and EdMPNTf$_2$N.

IL	Cation	Anion	Density (g cm^{-3})	Viscosity (cP)	T_{mel} (°C)	T_{dec} (°C)	Conductivity (mS cm^{-1})
EMImBF$_4$			1.29 (25 °C)	34.0(25 °C)	15	280	12.0 (25 °C)
	V$_{ion}$(nm^3): 0.156	V$_{ion}$(nm^3): 0.073	1.26 (60 °C)	12.7(60 °C)			39.6 (60 °C)
EdMPNTf$_2$N			1.40 (25 °C)	75.8(25 °C)	−14	320	1.2 (25 °C)
	V$_{ion}$(nm^3): 0.198	V$_{ion}$(nm^3): 0.232					

itance, C (F g^{-1}), was calculated according to

$$C = \frac{2\left|Im(Z)\right|}{2\pi f \left[(Im(Z))^2 + (Re(Z))^2\right] m}$$

where f is the operating frequency (Hz), Im(Z) and Re(Z) are the imaginary and real parts of the total device resistance (Ohm), and m is the mass of carbon in each electrode (g).

Galvanostatic charge–discharge cycle tests (GC) were measured using an Arbin BT-2000 testing system (Arbin Instruments, USA) in the voltage range 0–2.3 V and at charge–discharge current densities between 0.1 and 20 A g^{-1}, based on the mass of a single electrode. The gravimetric capacitance, C (F g^{-1}), was calculated according to

$$C = \frac{2I}{(dV/dt)m}$$

where I is the current (A), dV/dt is the slope of the discharge curve (V s^{-1}), and m is the mass of carbon in each electrode (g).

To perform high temperature electrochemical testing, the model capacitors were kept at 60 °C using an environmental test chamber (Tenney Environmental, Thermal Products Solutions, USA).

3. Results and discussion

3.1. Scanning electron microscope (SEM) of samples

Grinding the synthesized carbon samples using a ball mill resulted in the carbon powder with irregular morphology and the particle size of ~1–15 μm with most of the particles in the range of 3–7 μm (Fig. 1). Particles smaller than 1 μm were also present but their total volume was less than 5%, according to the SEM image analysis (Fig. 1). The small particle size can promote the electrolyte diffusion by providing a short ion-transport pathway [12]. The activation with CO$_2$ has not changed the particle shape and the particle size distribution to any significant extent (Fig. 1b).

3.2. Surface structural properties

A series of carbons with different pore structures were prepared by varying the activation condition. To understand the influence of activation time on the development of pore structure in the carbons, the investigated carbons were characterized by N$_2$ adsorption/desorption analyses. The N$_2$ sorption isotherms collected at

77 K on sucrose derived carbons are shown in Fig. 2a. It can be seen that the carbon prepared at 700 °C without any activation (ASC-0 h) adsorbed less than 60 cm^3 g^{-1} of N$_2$ at 0.99 of the relative pressure (P/P_0, where P_0 is the saturation vapor pressure of N$_2$ at 77 K). With increasing the activation time, the total pore volume (as calculated by measuring the amount of N$_2$ adsorbed at 0.99 P/P_0) increases gradually (Fig. 2a, Table 2). According to the classification of the International Union of Pure and Applied Chemistry (IUPAC), carbon samples exhibited type I isotherms with no hysteresis in the
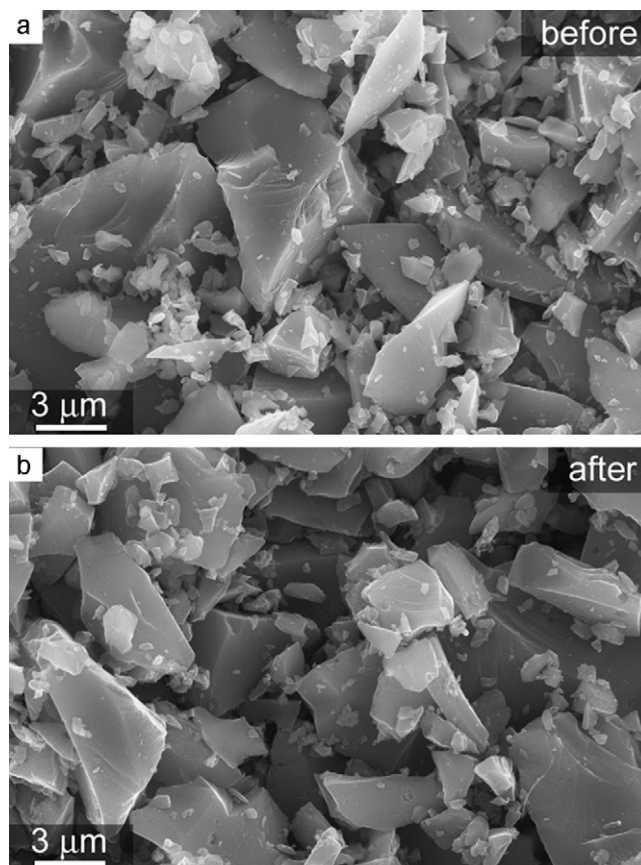
Fig. 1. Scanning electron microscopy micrographs of porous sucrose-derived carbon powder before (a) and after (b) CO$_2$ activation.
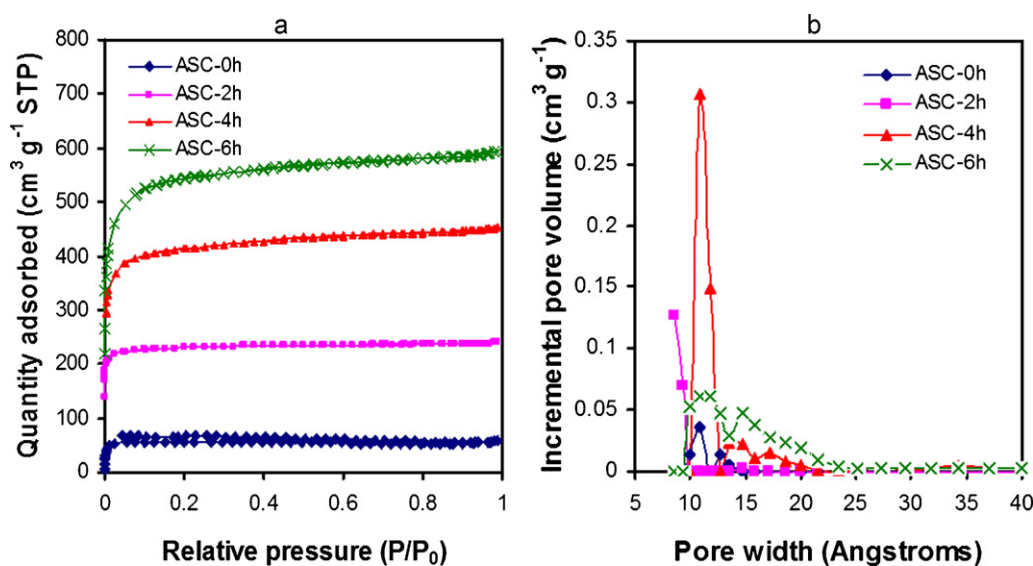
Fig. 2. (a) N_2 adsorption/desorption isotherms and (b) pore size distribution in the range of 10–40 Å for sucrose derived carbons activated for 0–6 h in the CO_2 stream at 900 °C.

adsorption/desorption isotherms, which is characteristic of microporous materials. However, the continued slope of the isotherms for ASC-4 h and ASC-6 h above a relative pressure of 0.3 suggests increase in the average pore size and the presence of larger micropores and small-sized mesopores in these activated carbons. The hysteresis loops in these samples are very modest, without a clear "knee" visible, suggesting that the effects of capillary condensation are not pronounced and that even the largest pores are smaller than 4–5 nm [38]. The N_2 sorption data are summarized in Table 2. Similarly to the pore volume changes, the SSA of the ACs increase with the CO_2 activation time and ASC-6 h demonstrates SSA as high as 1941 $m^2\,g^{-1}$ (Table 2).

The DFT pore-size distribution in Fig. 2b shows that with the increasing of CO_2 activation time, the pore-size of sucrose derived carbons becomes larger. Yet, the pore size distribution is relatively narrow and only a tiny fraction of mesopores appear when the activation time exceeds 4 h (Table 2). The appearance of larger pores is beneficial to the fast diffusion of large ions in ILs.

3.3. Electrochemical measurements

The specific capacitance of ASCs in EMImBF$_4$ and EdMPNTf$_2$N has been estimated using cyclic voltammetry (CV) at a scan rate of 1 mV s^{-1} (Fig. 3). It can be seen that there is an evident porosity effect on the shape CV curves. The as-produced (not shown) and 2 h activated sample (ASC-2 h) show relatively small specific capacitance even at an elevated temperature of 60 °C. The poor electrochemical performance of ASC-2 h cannot be explained only by its low surface area and low pore volume, particularly in the case of EdMPNTf$_2$N electrolyte (Table 2), and is likely resulted from the presence of bottle-neck pores, which were at least partially accessible by N_2 molecules in gas sorption experiments (Fig. 2a), but

blocked the transport of larger anions of ILs into the bulk of the carbon particles. The smaller anions in EMImBF$_4$ allowed larger specific capacitance to be achieved in ASC-2 h, particularly at 60 °C, when the viscosity of this IL is significantly reduced and its ionic conductivity is increased, as compared to its characteristics at room temperature (Table 1).

With the increasing of activation time, the specific capacitance of carbon samples increases greatly, with ASC-6 h sample showing nearly rectangular shape of the CV curve even at room temperature, which is characteristic of an ideal EDLC. The pseudocapacitance peaks visible at 1.2–1.8 V in the symmetrical EDLC (Fig. 3a and b) may result either from impurities present in the IL or from the reaction of the IL with the oxygen-containing functional groups on the carbon surface, induced by the activation process. The relatively large specific capacitance (in excess of 170 F g^{-1} in EdMPNTf$_2$N electrolyte) and rather good rate capability of the ASC-6 h electrodes have likely resulted from the large SSA, high percentage of micropores [14] (Table 2) and possibly smaller content of pore bottle-necks obtained by a prolonged activation. The larger micropores appearing in ASC with prolonged activation, of which the presence is suggested by the changes in the shape of the N_2 isotherms (Fig. 2a), must have allowed faster ion transport and higher achievable specific capacitance. The significant changes in the performance between the ASC-4 h and ACS-6 h samples in EdMPNTf$_2$N suggest that 6 h activation is needed for most of the bottle-neck pores to approach or exceed the dimension of the ions.

At room temperature all samples present better capacitive behaviors in EMImBF$_4$ than in EdMPNTf$_2$N due to the lower viscosity and higher ionic conductivity of EMImBF$_4$ combined with larger ion size in EdMPNTf$_2$N (Table 1). As expected, the specific capacitances of all the samples get better at higher temperature, due to increase in ionic mobility [39].

Table 2
Surface structural properties of activated sucrose derived carbons.

Sample	S_{BET} [a] ($m^2\,g^{-1}$)	V_P [b] ($cm^3\,g^{-1}$)	V_{micro} ($cm^3\,g^{-1}$)	V_{meso} ($cm^3\,g^{-1}$)
ASC-0 h	198.9250	0.091364	0.085100	0.00490
ASC-2 h	817.1116	0.373202	0.367412	0.00579
ASC-4 h	1473.7090	0.702511	0.653761	0.04875
ASC-6 h	1941.0791	0.919205	0.874515	0.04469

[a] BET surface area.
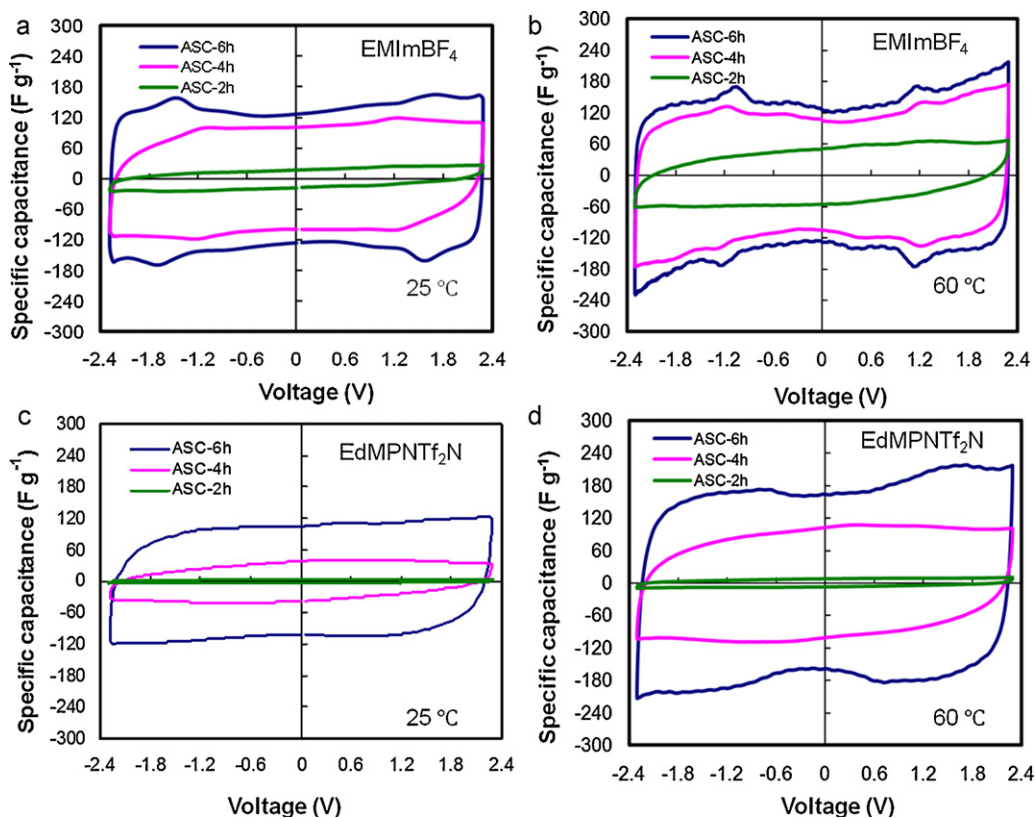[b] Total pore volume, measured at $P/P_0 = 0.99$.

Fig. 3. Cyclic voltammetry of activated sucrose derived carbons at a scan rate of 1 mV s^{-1} in ionic liquids: (a) in EMImBF$_4$ at 25 °C, (b) in EMImBF$_4$ at 60 °C, (c) in EdMPNTf$_2$N at 25 °C and (d) in EdMPNTf$_2$N ionic liquid at 60 °C.
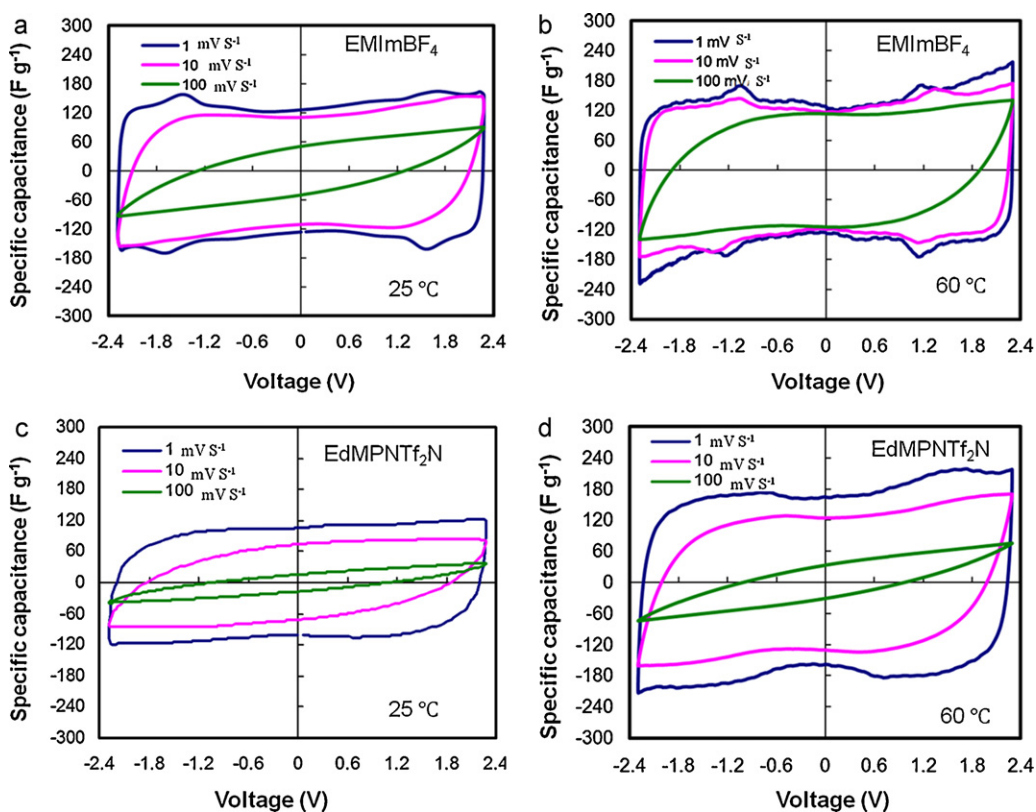

Fig. 4. Cyclic voltammetry of ASC-6 h at different scan rates: (a) in EMImBF$_4$ at 25 °C, (b) in EMImBF$_4$ at 60 °C, (c) in EdMPNTf$_2$N at 25 °C and (d) in EdMPNTf$_2$N ionic liquid at 60 °C.
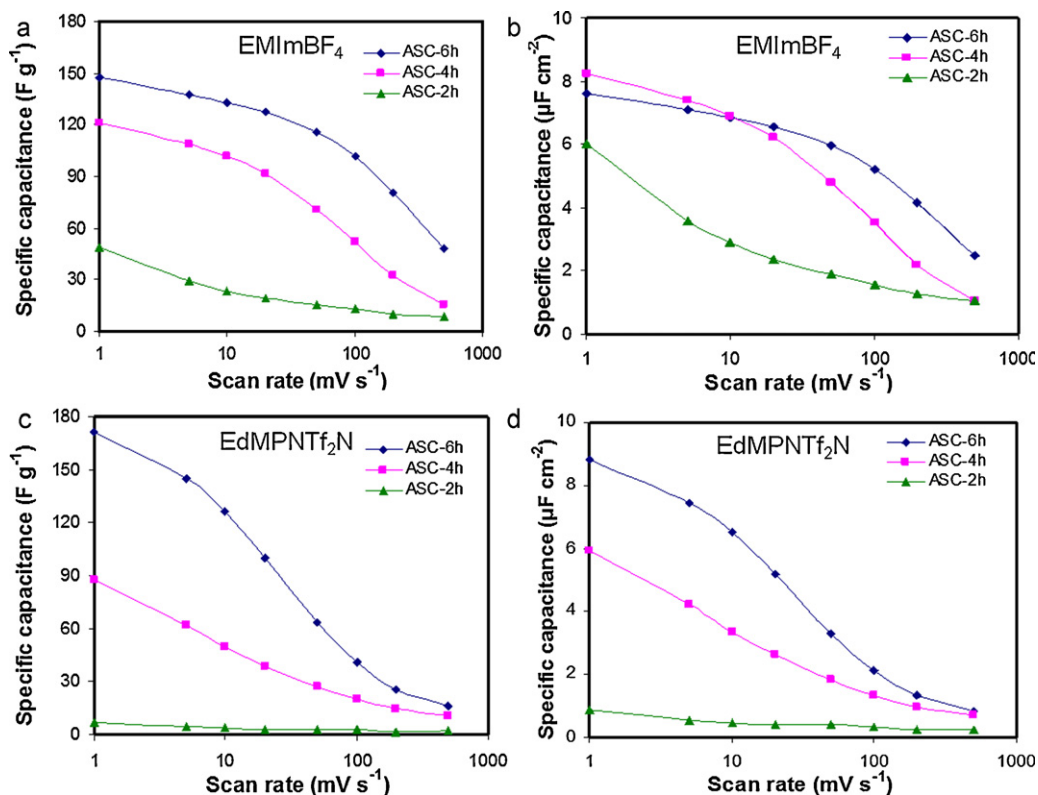
Fig. 5. Influence of scan rate on specific capacitance of activated sucrose derived carbons at 60 °C in: (a and b) EMImBF$_4$ and (c and d) EdMPNTf$_2$N ionic liquids.

Fig. 4 shows the CV curves of ASC-6 h in ILs at variable temperature. At room temperature, ASC-6 h possesses better capacitive behavior in EMImBF$_4$ than in EdMPNTf$_2$N in both low scan rate ($1\,\mathrm{mV\,s^{-1}}$) and high scan rate ($100\,\mathrm{mV\,s^{-1}}$). When the temperature increases to 60 °C, the performance of EdMPNTf$_2$N improves significantly. In fact, in spite of the larger ions, this IL surprisingly demonstrates even slightly higher specific capacitance than EMImBF$_4$ at a low scan rate of $1\,\mathrm{mV\,s^{-1}}$, presumably due to nanoconfinement effects previously discussed [9] and possibly closer approach of its asymmetric anions to the carbon pore walls. But when the scan rate is increased to $100\,\mathrm{mV\,s^{-1}}$, the slow ion transport of EdMPNTf$_2$N within the micropores causes significant distortion in the shape of the curve (Fig. 4d). Large pores or higher temperatures must be required to improve the EdMPNTf$_2$N-based

EDLC characteristics. Yet, the performance of ASC-6 h in EMImBF$_4$ at 60 °C is quite remarkable in spite of the absence of mesopores (Fig. 2), moderately large particle size and relatively thick ($\sim$300 μm) electrodes. Such characteristics suggest a promise of ASC materials for the applications in high-power EDLCs.

Fig. 5 summarizes the results discussed above and plots the influence of scan rates on specific capacitances of the investigated samples at 60 °C. The presented specific capacitances of the ASC samples at different scan rates were calculated from the CV and S_{BET} data. EDLC with ASC-6 h electrodes in EdMPNTf$_2$N shows the highest specific capacitance ($172\,\mathrm{F\,g^{-1}}$ at $1\,\mathrm{mV\,s^{-1}}$), while EDLC with ASC-6 h electrodes in EMImBF$_4$ shows the highest capacitance retention and the best rate performance among the tested devices. Indeed, with scan rate increasing from $1\,\mathrm{mV\,s^{-1}}$ to $500\,\mathrm{mV\,s^{-1}}$, the
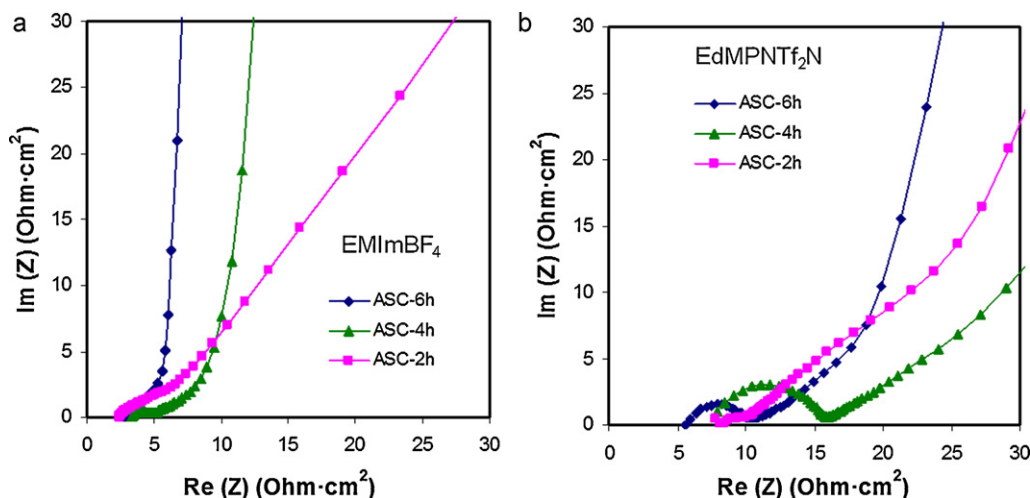

Fig. 6. Electrochemical impedance spectroscopy of activated sucrose derived carbons measured from 10^5 to 10^{-3} Hz at 60 °C in (a) EMIMBF$_4$ and (b) EdMPNTf$_2$N ionic liquids.
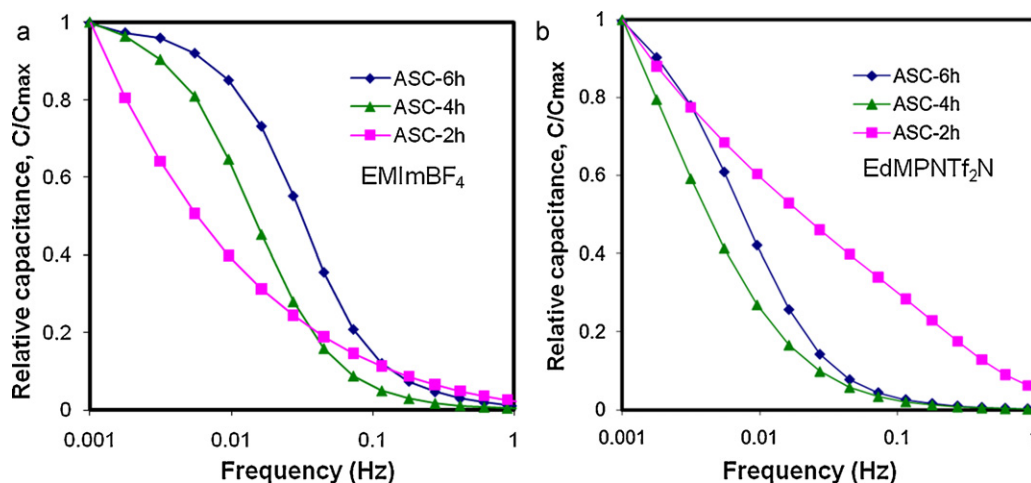
Fig. 7. Capacitance frequency response of activated sucrose derived carbons measured at 60 °C in (a) EMImBF$_4$ and (b) EdMPNTf$_2$N ionic liquids.

specific capacitances of ASC-6 h in EMImBF$_4$ gradually decreases from 148 F g^{-1} to 48 F g^{-1} (Fig. 5a) while the specific capacitances of ASC-6 h in EdMPNTf$_2$N decreases from 172 F g^{-1} to as low as 16 F g^{-1} (Fig. 5c) Interestingly, at slow scan rates the specific capacitance normalized by the surface area is slightly higher for ASC-4 h than for ASC-6 h samples in EMImBF$_4$ (Fig. 5b). This may be explained by the previously discussed hypothesis that larger normalized capacitance in IL can be achieved in pores with dimensions approaching (slightly larger) the size of the cations [9].

The electrochemical impedance behaviors of the investigated carbons in ILs are shown in Fig. 6. Except for ASC-2 h, the Nyquist plots of ASC-4 h and ASC-6 h in EMImBF$_4$ exhibit the typical features of porous electrodes with a relatively short 45° Warburg region at high-medium frequencies, and an almost vertical line at low frequencies, where the behaviors become mainly capacitive. The 45° segment in the Nyquist plot is related to the diffusion of the ions into the bulk of the electrode particles [40]. The increased length of this segment observed in EDLC with EdMPNTf$_2$N electrolyte, indicates an increased resistance faced by the larger ions during their transport in the micropores into the particle core. With increase in the activation time the length of this segment decreases (Fig. 6), in accord with previous measurements (Figs. 3–5). Additionally, ASC-4 h and ASC-6 h show semicircles at high frequencies in EdMPNTf$_2$N. The origin of such semicircles could be related to the contact resistance value between the Al current collector and carbon particles [39]. However, no analogous semicircles were observed in EMImBF$_4$ (Fig. 6a), even though the same Al current collector and carbon electrodes were used. We notice that the semicircles noticeably depend on the viscosity and conductivity of the electrolyte, supporting previous observations by Kurig et al. [41], and are more pronounced in samples activated for 4 and 6 h (Fig. 6b). If the contact between the current collector and the electrode is still responsible for the parasitic semicircle (equivalent circuit will consist of an additional small capacitance in parallel with small resistance prior to a classical EDLC circuit, represented by a transmission line [40]), it must be affected by the interaction between the functional groups on the C surface and IL electrolyte.

The equivalent series resistance (ESR), as determined by the intersection of the Nyquist plot with the *x*-axis (real part of the impedance) does not change significantly among the activated electrode samples (Fig. 6) because it is largely related to the ionic conductivity of electrolyte (electrical resistance of the electrodes is smaller than 0.4 Ω cm^2). As expected, ESR of EDLC with EdMPNTf$_2$N electrolyte, having lower ionic conductivity at this elevated temperature, is higher than that of EDLC with EMImBF$_4$ electrolyte.

The capacitance frequency response of the sucrose derived carbons with different activation time in ILs is presented in Fig. 7. If we approximate the highest operating frequency as the frequency at which the capacitance is 50% of its maximum value ($C/C_{max} = 0.5$), then ASC-6 h shows the highest operating frequency (characteristic charging/discharging time of 20 s), supporting previous measurements (Figs. 3–6). The improvements in the charge/discharge kinetics must be related to pore widening (Fig. 2b) and elimination of the narrow bottle-neck pores.

The influence of current density on specific capacitance for the most promising carbon electrode sample, ASC-6 h, is shown in Fig. 8. The specific capacitances at increasing current loads (from 100 mA g^{-1} to 20 A g^{-1}) were calculated from galvanostatic charge/discharge cycling curves, in which the data were measured at 60 °C that is commonly met in HEV applications [6]. Similarly to previous measurements (Fig. 5), at low current densities (<1 A g^{-1}) ASC-6 h in EdMPNTf$_2$N shows higher specific capacitance, but when the current density increases, the specific capacitance rapidly drops to 28 F g^{-1} at 5 A g^{-1} (Fig. 8). In contrast, ASC-6 h in EMImBF$_4$ consistently shows much better capacity retention (compare Figs. 5, 7 and 8). ASC-6 h retains 106 F g^{-1} at a very high current density of 10 A g^{-1} in EMImBF$_4$, 80% of that measured at 100 mA g^{-1}. However, further increase in the current density to 20 A g^{-1} leads to significant reduction in the effective capacitance (46 F g^{-1}).

Interestingly, the performance of ASC has been found superior to that previously reported in many mesoporous porous carbons. For example, the sucrose derived carbon synthesized in the pores
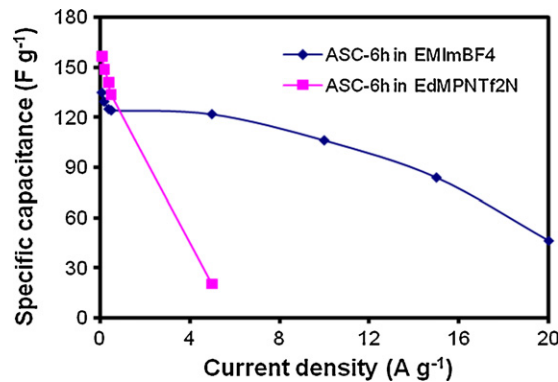

Fig. 8. Influence of current density on specific capacitance of sample ASC-6 h in different ILs at 60 °C.

of the sacrificial 3D mesoporous silica SBA-15 with ordered pores showed moderate specific capacitance of $125 \, F \, g^{-1}$ capacitance in $EMImBF_4$ at a low current density. At higher current density of only $4 \, A \, g^{-1}$, the specific capacitance dropped to $\sim 40 \, F \, g^{-1}$ [42,43]. The mesoporous carbons prepared from barium citrates [42] also showed an impressive gravimetric specific capacitance of $170 \, F \, g^{-1}$ in $EMImBF_4$. Yet, as the current density increases to $10 \, A \, g^{-1}$, the effective specific capacitance drops to only $41.3 \, F \, g^{-1}$ (24% capacitance retention). In contrast, ASC-6 h with smaller pores and a narrow pore size distribution, exhibits greater rate performance and capacitance retention ability. We propose that a long time activation (6 h) by CO_2 eliminates the bottle-neck pores and facilitates ion transport through the carbon particle pore network at fast charge–discharge rates.

4. Conclusions

Microporous carbons were prepared by pyrolysis of sucrose at $900 \, °C$ and its subsequent activation with CO_2. The surface area and pore volume was found to increase with the activation time and reach $1941 \, m^2 \, g^{-1}$ and $0.92 \, cm^3 \, g^{-1}$ for 6 h activation. The electrochemical performance of the produced samples was evaluated in two kinds of ILs, $EMImBF_4$ and $EdMPNTf_2N$. The CV measurements showed the carbon sample activated for 6 h (ACS-6 h) to reach the specific capacitances of $172 \, F \, g^{-1}$ in $EdMPNTf_2N$ and $148 \, F \, g^{-1}$ in $EMImBF_4$, respectively. The $EMImBF_4$ allowed better rate performance to be achieved. The characteristic charge discharge time for ACS-6 h in $EMImBF_4$ was estimated to be as low as 20 s. This sample also showed excellent capacity retention. At $10 \, A \, g^{-1}$ this sample retained over, 80% of its maximum capacitance (measured at $100 \, mA \, g^{-1}$) in our charge–discharge tests performed at $60 \, °C$. The performed tests suggest that in spite of their small pore size, activated sucrose derived carbons show great promise as a low-cost renewable electrode material for applications in EDLCs with IL electrolytes.

Acknowledgment

References

[1] P. Simon, Y. Gogotsi, Nat. Mater. 7 (2008) 845–854.
[2] E. Frackowiak, F. Beguin, Carbon 39 (2001) 937–950.
[3] P.F. Ribeiro, B.K. Johnson, M.L. Crow, A. Arsoy, Y. Liu, Proc. IEEE 89 (2001) 1744–1756.
[4] P. Sharma, T.S. Bhatti, Energy Convers. Manage. 51 (2010) 2901–2912.
[5] I. Kovalenko, D. Bucknall, G. Yushin, Adv. Funct. Mater. 20 (2010) 3979–3986.
[6] M. Lazzari, F. Soavi, M. Mastragostino, J. Electrochem. Soc. 156 (2009) A661–A666.
[7] H. Kurig, A. Janes, E. Lust, J. Electrochem. Soc. 157 (2010) A272–A279.
[8] M. Lazzari, F. Soavi, M. Mastragostino, J. Power Sources 178 (2008) 490–496.
[9] C. Largeot, C. Portet, J. Chmiola, P.L. Taberna, Y. Gogotsi, P. Simon, J. Am. Chem. Soc. 130 (2008) 2730–2731.
[10] T. Sato, G. Masuda, K. Takagi, Electrochim. Acta 49 (2004) 3603–3611.
[11] A. Balducci, R. Dugas, P.L. Taberna, P. Simon, D. Plée, M. Mastragostino, S. Passerini, J. Power Sources 165 (2007) 922–927.
[12] A. Balducci, W.A. Henderson, M. Mastragostino, S. Passerini, P. Simon, F. Soavi, Electrochim. Acta 50 (2005) 2233–2237.
[13] S. Shiraishi, N. Nishina, A. Oya, R. Hagiwara, Electrochemistry 73 (2005) 593–596.
[14] J. Chmiola, G. Yushin, Y. Gogotsi, C. Portet, P. Simon, P.L. Taberna, Science 313 (2006) 1760–1763.
[15] J. Chmiola, G. Yushin, R. Dash, Y. Gogotsi, J. Power Sources 158 (2006) 765–772.
[16] E. Raymundo-Piñero, K. Kierzek, J. Machnikowski, F. Béguin, Carbon 44 (2006) 2498–2507.
[17] Y. Korenblit, M. Rose, E. Kockrick, L. Borchardt, A. Kvit, S. Kaskel, G. Yushin, ACS Nano 4 (2010) 1337–1344.
[18] A. Kajdos, A. Kvit, F. Jones, J. Jagiello, G. Yushin, J. Am. Chem. Soc. 132 (2010) 3252.
[19] C. Portet, Z. Yang, Y. Korenblit, Y. Gogotsi, R. Mokaya, G. Yushin, J. Electrochem. Soc. 156 (2009) A1–A6.
[20] D. Hulicova-Jurcakova, M. Seredych, G. Lu, T.J. Bandosz, Adv. Funct. Mater. 19 (2009) 438–447.
[21] D. Hulicova-Jurcakova, M. Kodama, S. Shiraishi, H. Hatori, Z. Zhu, G. Lu, Adv. Funct. Mater. 19 (2009) 1800–1809.
[22] D. Hulicova-Jurcakova, M. Kodama, H. Hatori, Chem. Mater. 18 (2006) 2318–2326.
[23] C.O. Ania, V. Khomenko, E. Raymundo-Piñero, J.B. Parra, F. Béguin, Adv. Funct. Mater. 17 (2007) 1828–1836.
[24] H. Benaddi, T.J. Bandosz, J. Jagiello, J.A. Schwarz, J.N. Rouzaud, D. Legras, F. Béguin, Carbon 38 (2000) 669–674.
[25] C. Portet, G. Yushin, Y. Gogotsi, J. Electrochem. Soc. 155 (2008) A531–A536.
[26] A. Lewandowski, M. Galinski, J. Phys. Chem. Solids 65 (2004) 281–286.
[27] W. Lu, L. Qu, K. Henry, L. Dai, J. Power Sources 189 (2009) 1270–1277.
[28] H. Zhang, G. Cao, Y. Yang, Z. Gu, Carbon 46 (2008) 30–34.
[29] E.N. Hoffman, G. Yushin, T. El-Raghy, Y. Gogotsi, M.W. Barsoum, Micropor. Mesopor. Mater. 112 (2008) 526–532.
[30] Z.G. Cambaz, G.N. Yushin, Y. Gogotsi, K.L. Vyshnyakova, L.N. Pereselentseva, J. Am. Ceram. Soc. 89 (2006) 509–514.
[31] C. Portet, P.L. Taberna, P. Simon, E. Flahaut, C. Laberty-Robert, Electrochim. Acta 50 (2005) 4174–4181.
[32] G. Salitra, A. Soffer, L. Eliad, Y. Cohen, D. Aurbach, J. Electrochem. Soc. 147 (2000) 2486–2493.
[33] V. Subramanian, C. Luo, A.M. Stephan, K.S. Nahm, S. Thomas, B. Wei, J. Phys. Chem. C 111 (2007) 7527–7531.
[34] K. Kadirvelu, M. Kavipriya, C. Karthika, M. Radhika, N. Vennilamani, S. Pattabhi, Bioresour. Technol. 87 (2003) 129–132.
[35] T.Y. Zhang, W.P. Walawender, L.T. Fan, M. Fan, D. Daugaard, R.C. Brown, Chem. Eng. J. 105 (2004) 53–59.
[36] C. Schreiner, S. Zugmann, R. Hartl, H.J. Gores, J. Chem. Eng. Data 55 (2010) 1784–1788.
[37] I. Krossing, J.M. Slattery, C. Daguenet, P.J. Dyson, A. Oleinikova, H. Weingärtner, J. Am. Chem. Soc. 128 (2006) 13427–13434.
[38] R.T. Yang, Adsorbents: Fundamentals and Applications, Wiley & Sons, Inc., Hoboken, NJ, USA, 2003.
[39] C. Portet, P.L. Taberna, P. Simon, E. Flahaut, J. Electrochem. Soc. 153 (2006) A649–A653.
[40] P.L. Taberna, P. Simon, J.F. Fauvarque, J. Electrochem. Soc. 150 (2003) A292–A300.
[41] H. Kurig, A. Jänes, E. Lust, J. Eletrochem. Soc. 157 (2010) A272–A279.
[42] J. Zhou, X. Yuan, W. Xing, W. Si, S. Zhuo, Carbon 48 (2010) 2765–2772.
[43] D. Zhao, J. Feng, Q. Huo, N. Melosh, G.H. Fredirckson, B.F. Chemlka, G.D. Stucky, Science 279 (1998) 548–552.